This article was published in Journal of Photochemistry and Photobiology A: Chemistry, 311, 41-52, 2015
http://dx.doi.org/10.1016/j.jphotochem.2015.06.007

Photocatalytic Oxidation of Gaseous Perchloroethylene over TiO_2 Based Paint

Ricardo A.R. Monteiro[1], Adrián M.T. Silva[2,*], Joana R.M. Ângelo[3], Gabriela V. Silva[4], Adélio M. Mendes[3], Rui A.R. Boaventura[1], Vítor J.P. Vilar[1,*]

[1]LSRE - Laboratory of Separation and Reaction Engineering
[2]LCM - Laboratory of Catalysis and Materials
Associate Laboratory LSRE/LCM
Faculdade de Engenharia, Universidade do Porto, Rua Dr. Roberto Frias, 4200-465 Porto, Portugal
[3]LEPABE - Laboratory for Process, Environment, Biotechnology and Energy Engineering
Faculdade de Engenharia, Universidade do Porto, Rua Dr. Roberto Frias, 4200-465 Porto, Portugal
[4]INEGI – Institute of Science and Inovation in Mechanical and Industrial Engineering
Faculdade de Engenharia, Universidade do Porto, Rua Dr. Roberto Frias, 4200-465 Porto, Portugal

[*] Authors to whom correspondence should be addressed:
Tel. +351 918257824; Fax: +351 225081674; E-mail addresses: adrian@fe.up.pt (Adrián M.T. Silva); vilar@fe.up.pt (Vítor J.P. Vilar).

Abstract

Perchloroethylene (PCE) is a volatile chlorinated compound persistently present in indoor air of several industrial closed facilities. Due to its environmental and human health impact, efforts have been directed in the last decades towards the degradation of this kind of air pollutants. The photocatalytic oxidation (PCO) of PCE was studied in an annular photoreactor equipped with a compound parabolic collector (CPC) and employing two different configurations of a monolithic structure of cellulose acetate coated with an active TiO_2-based paint (9 wt.% of TiO_2 PC500) under solar radiation. The influence of the experimental conditions, namely feed flow rate (Q_{feed}), initial concentration ($C_{PCE,\ feed}$), relative humidity (RH) in the system, absence of oxygen and incident irradiance on the PCE conversion was evaluated. Under the best experimental conditions ($C_{PCE,\ feed}$ = 1100 ppm, Q_{feed} = 75 $cm^3\ min^{-1}$, RH = 40 % and I = 38.4 $W_{UV}\ m^{-2}$ in the presence of oxygen) 60 % of the initial PCE concentration was converted. The results showed that depending on the configuration of the structure, photocatalytic degradation of PCE can be enhanced by approximately 58 %. Results obtained at low RH suggest that $Cl^{\bullet}$ radical chain propagation reactions may be included in the PCO mechanism of PCE. Also, in the absence of oxygen the photoreaction can still take place.

Keywords: Solar Photocatalysis; Air Decontamination; Perchloroethylene; Photocatalytic Paint; Cellulose Acetate Monolithic Structure

1. Introduction

Heterogeneous photocatalytic processes have been considered a good option for air and water decontamination, since they can operate at room temperature, uses atmospheric air as oxidant source, and solar radiation for the photonic activation of the photocatalyst (usually TiO_2 [1]), and are able to degrade/mineralize a wide range of recalcitrant organic pollutants into harmless or easily neutralized final products (CO_2, H_2O and mineral acids) [1-3]. In particular, a great deal of attention has been paid to the immobilization of UV-Vis active novel nanomaterials onto inert supports, avoiding the subsequent removal of the catalyst particles and make them resistant to mechanical abrasion and to environmental ageing without impairing their performance. In this sense, a substrate for the deposition of active nanomaterial's for gas-phase photocatalysis should have the following requirements [3]: *i*) promote good photocatalyst adherence; *ii*) be chemically inert; photo, chemical and mechanical-resistant; *iii*) transparent to UV radiation; *iv*) promote good flow rate distribution avoiding the formation of the dead volumes and the limitations of the mass transfer processes; *v*) high surface area; *vi*) good adsorption capability for the organic compounds to be degraded; *vii*) light weight and easy handling; *viii*) low cost.

TiO_2 has been incorporated into a wide range of construction materials such as, tiles [4, 5], paving blocks [6, 7], wall papers [8, 9] and paints [10-14], towards the improvement of air quality, self-cleaning and self-disinfecting agents. Among all construction materials, paints are especially attractive as support for photocatalytic active TiO_2 materials mainly due to the fact that almost all indoor and outdoor surfaces can be decorated with a thick and opaque film without impairing its photoactivity and obviously to aesthetic applications. Bygott et al. [10] conducted a field trial painting 300 m^2 of walls with a silicate-based paint incorporating 7.5 wt.% of photocatalytic TiO_2. The authors

reported a daily NO_x abatement of *ca.* 4.5 g in about 10 000 m^3 of air around school children playground [10]. Maggos et al. [12] stated a NO and NO_2 reduction of 19 % and 20 % respectively, using a white acrylic TiO_2-containing paint coated on the ceiling surface of a car – NO_x depollution tests were conducted in an artificially closed parking area polluted by a car exhaust during the testing period. Salthammer and Fuhrmann [13] tested two different types of commercially available wall paints in a 1 m^3 test chamber with and without air exchange using artificial sunlight. The results showed that formaldehyde was photo-oxidized under static conditions. But, for typical VOCs under dynamic conditions, no significant photocatalytic activity was observed. In another real-outdoor conditions study, Ângelo et al. [14] determined the NO photo-abatement efficiency of photocatalytic paints when irradiated by sunlight. The paints were applied in a fiber cement board with 70 × 20 cm^2 and a stable NO feed stream was fed to the photoreactor (C_{NO} = 100 ± 20 ppbv). The best performing paint tested was formulated with PC500 and calcium carbonate yielding *ca.* 95 % of NO conversion.

Although the promising results and potential application concerning photodegradation of air pollutants using TiO_2-based paints, only few studies can be found in the literature regarding their use in the degradation of chlorinated VOCs. In addition, this paper presents a study on gas-phase PCO of PCE over TiO_2 (when incorporated in a paint), using a lab-scale continuous-flow single-pass annular photoreactor equipped with a compound parabolic collector – CPC (instead of studying the paint as common construction material). In our previous work [15] we reported a large concentration of PCE in the indoor air of different stages of a wastewater treatment plant (WWTP), mainly associated with the aeration and mechanical agitation processes, as well as with the different sludge treatment stages. Considering its high toxicity and volatility and since it is suspected to be carcinogenic to humans and extremely persistent in the environment,

101 as well as to generate toxic reaction intermediates such as phosgene, chloroform and
102 carbon tetrachloride, PCE present in water and/or air must be removed. Two
103 configurations based on a monolithic structure of cellulose acetate were employed as
104 catalytic bed. Applying such structure in an annular reactor it is possible to take advantage
105 of the low pressure drop and high surface-area-to-volume ratio typical of monolithic
106 reactors [16] as well as to profit from the fact that the whole reactor and the catalytic bed
107 can be illuminated, enhancing the photonic efficiency [17]. Besides, the presence of an
108 internal cylinder allows the use of a UVA or solar light lamp which may enable
109 photocatalysis even at low or none natural irradiance conditions such as night and/or in
110 indoor environments [18, 19]. To the best of our knowledge, this is the first time that the
111 performance of TiO_2-based paints and their applicability on gas-phase photo-oxidation
112 processes for PCE abatement is evaluated. The photocatalytic oxidation (PCO) of PCE
113 was studied for different operating conditions, such as feed flow rate, PCE concentration,
114 relative humidity, absence of oxygen and incident irradiance. In addition, based on the
115 previous studies and on the experimental results obtained in the present work regarding
116 the intermediate compounds detected by GC-MS, a reaction mechanism was formulated.
117

118 **2. Experimental**

119 *2.1. Materials and chemicals*

120 TiO_2 photocatalyst PC500 (Cristal) was selected to modify a vinyl paint. This
121 choice was based on Águia et al. [20] works where is reported a water-based vinyl paint
122 loaded with TiO_2 photocatalyst PC500 (Cristal) that produced higher NO conversions
123 among several other commercially available photocatalysts and, thus, it was selected for
124 the studies shown in the present work. PC500 photocatalyst properties are detailed in Table
125 1.

126 Cellulose acetate monolithic structures (TIMax CA50-9/S – L_C = 80 mm,
127 d_{ch}^2 = 9 mm × 9 mm, $e_{w,ch}$ = 0.1 mm; Wacotech GmbH & Co. KG.) were used to
128 immobilize the photocatalytic paint. For the generation of humidified air streams
129 contaminated with PCE, deionized water and PCE (≥ 99.5 %; CAS no. 127-18-4; Panreac
130 Química S.A.U.) were used without further purification. Air Liquide provided all gases,
131 with minimum total purities of 99.999 %: helium N50, nitrogen N50, and synthetic air
132 N50 (O_2: 20 ± 1 %; H_2O: < 3 ppm; C_nH_m: < 0.1 ppm; CO_2: < 1 ppm; CO: < 1 ppm).
133
134 **Table 1.** TiO_2 PC500 and paint properties and photoreactor dimensions employed in the
135 gas-phase PCO of PCE under simulated solar radiation.

Catalyst and Paint [20]		
TiO_2	Manufacturer	PC500 (Cristal)
	Crystal structure	>99% anatase
	Crystal size [nm]	5-10
	Shape	Agglomerates
	Surface area [m^2 g^{-1}]	345
	Agglomerate size [µm]	1.2-1.7
	Shape	Agglomerates
Water-based vinyl paint (wet basis)	Pigmentary TiO_2	18 wt.%
	Water	30 wt.%
	Extenders ($CaCO_3$ and silicates)	18 wt.%
	Polymer extender slurry	8 wt.%
	Binder slurry	20 wt.%
	Additives (in slurry)	6 wt.%
Photoreactor		
Outer tube (Pyrex-glass)	$d_{ot,e}$ [cm]	5.00
	$d_{ot,i}$ [cm]	4.64
Inner tube (Pyrex-glass)	$d_{in,e}$ [cm]	2.00
	$d_{in,i}$ [cm]	1.64
Photoreactor	L_R [cm]	16.0
	V_R [cm^3]	220

136
137 *2.2. Photocatalytic films preparation and characterization*
138 The TiO_2 PC500 catalyst and water-based vinyl paint properties are summarized
139 in Table 1. From the original water-based vinyl paint, half of the pigmentary TiO_2 (9 wt.%

140 in wet base) was removed; the photocatalytic paint (henceforth named as P) was,
141 subsequently, formulated by adding 9 wt.% of TiO_2 PC500 (*ca.* 50 cm^3 of paint without
142 50 % of pigmentary TiO_2 and mixing for 30 min at 300 rpm in a 100 cm^3 stainless steel
143 vessel), as reported by Águia et al. [11]. The final TiO_2 PC500 and pigmentary TiO_2
144 content was 9 wt.% in wet basis (*ca.* 18 wt.% in dry basis) (see Table 1).

145 Sets of cellulose acetate monolithic structures (C) were coated with a thin film of
146 the photocatalytic paint using the dip-coating method (Dip-Coater RDC21-K, Bungard
147 Elektronik GmbH & Co. KG.). Prior to dip-coating, cellulose acetate monolithic
148 structures were immersed for 1 h in distilled water and alkaline detergent (Derquim LM
149 01, Panreac Química, S.A.U.), subsequently rinsed exhaustively with Milli-Q water, and
150 finally, dried at 323 K. Afterwards, layers of photocatalytic paint were dip-coated at a
151 withdrawal rate of 0.8 mm s^{-1} until a thin and uniform film with different thicknesses was
152 formed on each substrate surface (these samples were dried at 323 K for 1 h between each
153 layer deposition). The photocatalytic paint immobilized (P) on different sets of cellulose
154 acetate monolithic structures was labelled as xPCy, where x refers to the number of layers
155 coated and y is 1 for configuration 1 and 2 for configuration 2.

156 Scanning electron microscopy (SEM) coupled with energy dispersive X-ray
157 (EDX) analysis was performed in a FEI Quanta 400 FEG ESEM / EDAX Genesis X4M
158 apparatus equipped with a Schottky field emission gun (for optimal spatial resolution) for
159 the determination of the cross-section of selected photocatalytic paint films. These
160 SEM/EDX analyses were made at CEMUP (Centro de Materiais da Universidade do
161 Porto).

162

2.3. Experimental setup

The experimental setup is schematized in Fig. 1. A full description of the whole apparatus is given elsewhere [21]. The humid air stream contaminated with PCE was generated by feeding controlled flow rates of air (mass flow controllers from Bronkhorst High-Tech B.V., El-Flow, precision ± 1 % FS) to two Woulff bottles (Normax, Lda.), one containing PCE and another filled with deionized water (Fig. 1a). The humidified and contaminated air streams are then mixed with a controlled flow rate of dry air for producing the desirable feed composition.

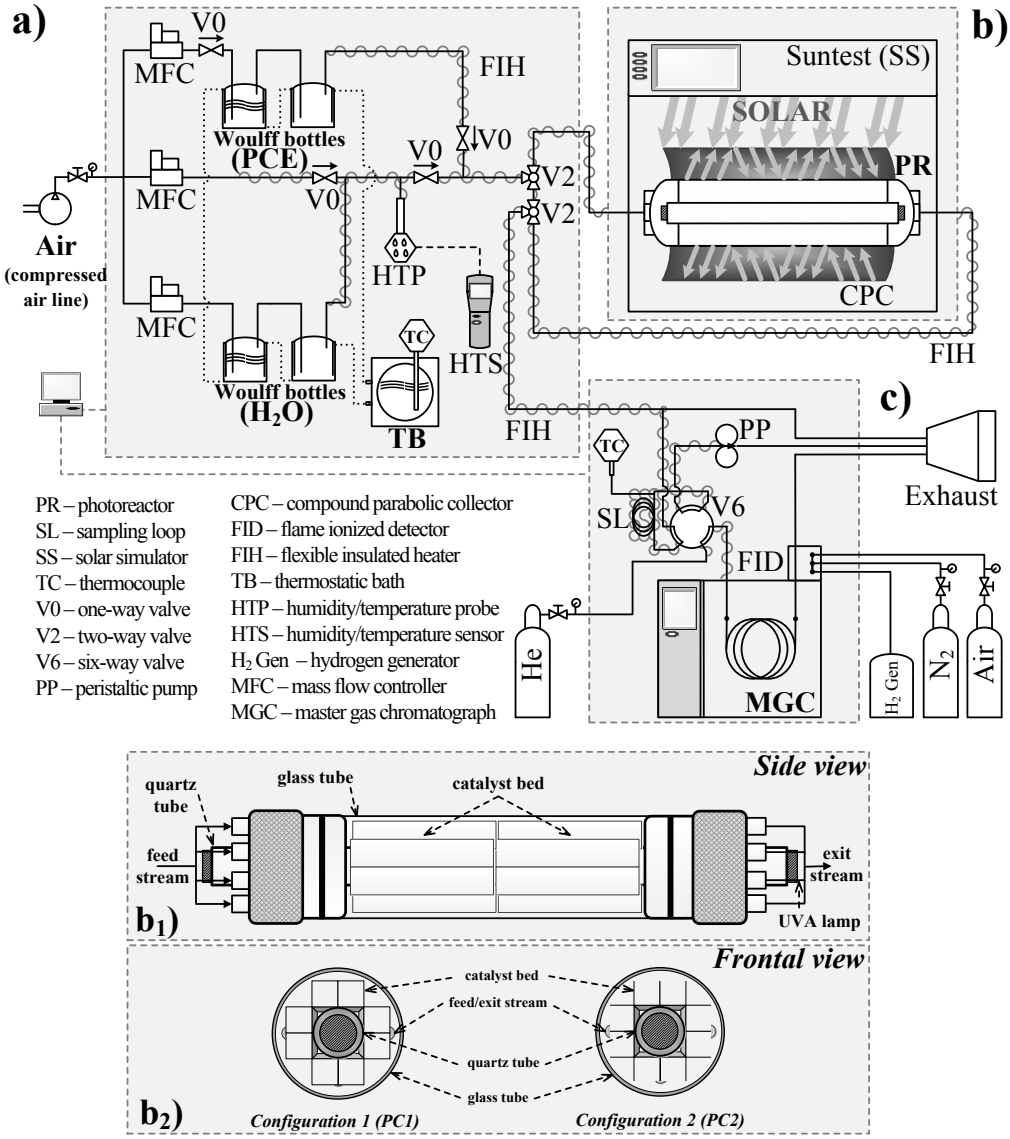

Fig. 1. Experimental set-up and the annular photoreactor schematic representation: a) lab-scale unit used for the generation of air streams containing PCE and water vapour; b)

174 sunlight simulator containing the photoreactor: b_1) side view b_2) frontal view of the two
175 configurations used; c) master gas chromatograph analytic system used for the analysis
176 of the photoreactor feed and exit streams.
177

178 For the oxygen-free experiments the air stream was replaced by N_2 stream and the
179 deionized water inside the Woulff bottle was replaced by a 10 g L^{-1} Na_2SO_3 solution in
180 order to remove any dissolved O_2 present in the water. The photocatalytic system consists
181 of four parts (Fig. 1b): i) a solar simulator (Atlas, model Suntest XLS+) with 0.110 m^2 of
182 working area illuminated by a 1.7 kW air-cooled xenon arc lamp and an infrared coated
183 quartz glass daylight filter; ii) a compound parabolic collector (CPC) with 0.023 m^2 of
184 illuminated area with electropolished anodized aluminium reflectors assuring that the
185 whole reactor is illuminated [17]; iii) a photoreactor consisting of two concentric and
186 axially centred tubes (both tubes made of soda-lime glass, Duran borosilicate glass 3.3,
187 cut-off at 280 nm, Schott-Rorhglas GmbH); iv) an actinic lamp (Actinic BL TL 6 W,
188 Koninklijke Philips Electronics N.V.) for catalyst degassing and activation purposes,
189 placed inside and axially centred in the inner tube (peak at 365 nm – UVA radiation).
190 Table 1 summarizes the tube dimensions of the photoreactor and Figs. $1b_1$ and $1b_2$
191 schematically represent the side and frontal views of the annular photoreactor,
192 respectively.

193 PCE concentration histories were monitored using a gas chromatograph (MGC
194 Fast GC, Dani Instruments S.p.A.) equipped with a flame ionisation detector (FID) and a
195 Volcol capillary column (20 m × 0.18 mm × 1.00 μm; Supelco, Sigma-Aldrich Co. LLC.)
196 (see Fig. 1c). The experimental setup was connected to a computer and controlled using
197 a data acquisition board system and an in-house program developed routine written in
198 Labview environment (NI Corporation). All connections are of 1/16" stainless steel
199 tubing (Swagelok Company) to reduce dead volumes.

200 Additionally, intermediates formed from the PCE photo-oxidation were analysed
201 at steady-state, after collecting the photoreactor exit stream into a 5 L Tedlar bag
202 (232-05SKC, SKC Inc.) and transferring the sample to stainless steel tubes with Tenax
203 TA60/80 mesh (Supelco, Sigma-Aldrich Co. LLC.). The identification and quantification
204 of such products was conducted in a thermal desorption system (SDT 33.50, Dani
205 Instruments S.p.A.) working in line with a GC/MSD device (a gas chromatograph GC
206 6890N coupled to a mass spectrometer detector MSD 5973, Agilent Technologies, Inc.).
207 The response factor of toluene (ISO 16000-6 [22]) was used to determine the
208 concentration of the major products (while for PCE, specific response factor was used).
209

210 *2.4. Photocatalytic experiments*

211 All experiments were taken inside the chamber of the aforementioned solar
212 simulator, which can simulate the outdoor solar radiation within a spectral range of
213 $300 < \lambda < 800$ nm. The UV incident irradiance was measured using a broadband UV
214 radiometer (CUV 5, Kipp & Zonen B.V.), placed on the outside of the outer tube and at
215 the same height, within a spectral range of 280 to 400 nm corresponding to the UV
216 fraction of the solar radiation.

217 In order to evaluate the photolytic oxidation of PCE, the photoreactor was first
218 assembled with the uncoated cellulose acetate structure. Then, sets of xPC1 were prepared
219 in order to evaluate the influence of the coat thickness upon the photocatalytic activity.
220 After assessing the optimum coat thickness and considering that monolithic structures are
221 prone to shading effects owing not only to the structure itself but also to the coat thickness,
222 a second configuration, xPC2, where the outer walls were removed was tested
223 (configuration 2; see Fig. 1b$_2$). xPC2 coated with the same photocatalytic paint aiming at
224 a comparable paint surface density, ρ_A, between both configurations, was prepared in

225 order to clarify the influence of the configuration on the photocatalytic activity. The
226 further influence of the different operating conditions on the PCO of PCE was carried out
227 using the same set of xPC2. Table 2 summarizes the catalytic bed properties of all xPCy
228 used in this study and a schematic representation of both configurations employed in this
229 study can be found in Fig. $1b_2$.

Table 2. Catalytic bed characteristics and configurations employed in the gas-phase PCO of PCE under simulated solar radiation.

Catalytic bed (xPCy)								
Catalyst (P)	Pigmentary	9 wt.% (wet basis)						
	PC500	9 wt.% (wet basis)						
	ρ_P [mg cm^{-3}]	2.61						
Substrate (C)	ρ_{Cx} [mg cm^{-3}]	1.30						
	d_{ch} [cm]	0.9						
	Porosity *(ε)*	0.991						
Config.1 (xPC1)	A_{PC1} [cm^2]	806.4						
	n_{layers} [x]	1	3	4	7	9	10	12
	m_P [mg]	103.2	340.7	442.2	708.1	943.9	1022.8	1237.4
	m_{C1} [mg]	3.1609	3.2698	3.1939	3.1963	3.1739	3.3170	3.2418
	$\rho_{A,\,PC1}$ [mg cm^{-2}]	0.1280	0.4225	0.5484	0.8781	1.171	1.268	1.534
Config.2 (xPC2)	A_{PC2} [cm^2]	576.0						
	n_{layers} [x]	5						
	m_P [mg]	503.6						
	m_{C1} [mg]	2.0657						
	$\rho_{A,\,PC2}$ [mg cm^{-2}]	0.8743						

232 The efficiency of the process was expressed in terms of PCE conversion and

233 calculated as follows:

234 $$\text{Conversion (\%)} = \left(1 - \frac{C_{\text{PCE, exit}}}{C_{\text{PCE, feed}}}\right) \times 100 \qquad \text{(eq. 1)}$$

235 where $C_{\text{PCE, feed}}$ and $C_{\text{PCE, exit}}$ are the PCE concentration (in ppm) on the feed and exit

236 streams, respectively. Several experimental conditions were employed aiming the study

237 of PCO of PCE: feed flow rate (75–300 cm^3 min^{-1}, measured at 1 bar and 298 K), PCE

238 concentration (600 - 2200 ppm), relative humidity (3 – 40 %, measured at 1 bar and

239 298 K), relative humidity in the absence of oxygen (3 - 40 %, measured at 1 bar and

240 298 K) and incident UV irradiance (18.9 - 38.4 W_{UV} m^{-2}, measured for the spectral range

241 between 280 - 400 nm: UV fraction of the incident sunlight). Table 3 summarizes all the

242 experimental conditions.

243

244 **Table 3.** Experimental conditions employed in the study of PCE photodegradation

Run	Q_{feed}* [cm^3 min^{-1}]	$C_{PCE, feed}$ [ppm]	RH* [%]	I# [W m^{-2}]
1[a)], 2[a)], 3[a)]	75	1100	40	38.4, 29.1, 18.9
4[b)], 5, 6	150	1100	40	38.4, 29.1, 18.9
7, 8, 9	300	1100	40	38.4, 29.1, 18.9
10, 11, 12	150	600	40	38.4, 29.1, 18.9
13, 14, 15	150	2200	40	38.4, 29.1, 18.9
16, 17, 18	150	1100	20	38.4, 29.1, 18.9
19, 20, 21	150	1100	3	38.4, 29.1, 18.9
22[c)], 23[c)], 24[c)]	150	1100	40	38.4, 29.1, 18.9
25[c)] 26[c)] 27[c)]	150	1100	20	38.4, 29.1, 18.9
28[c)] 29[c)] 30[c)]	150	1100	3	38.4, 29.1, 18.9

* Measured at 298 K and 1 bar.
# Measured within 280 – 400 nm (sunlight UV fraction).
a) Experimental conditions employed in the experiments for evaluation of the effect of number of layers and structure configuration on photocatalytic conversion.
b) Experimental conditions used for photolysis experiment and for collecting the outlet gas stream at steady state after PCE degradation.
c) Experimental conditions employed for oxygen free experiments.

245

246 Prior to the experiments, the catalytic bed was degassed and the photocatalytic paint coat
247 activated under UVA radiation and by flowing 30 cm^3 min^{-1} (measured at 1 bar and
248 298 K) of synthetic air with 40 % of relative humidity for 24 h as described elsewhere
249 [11]. Before turning on the sunlight simulator, the PCE concentration in the feed stream
250 was measured at the by-pass (see Fig. 1a) until steady-state was reached. Then, the by-
251 pass to the photoreactor was cancelled and the gas stream was redirected to the
252 photoreactor. The feed composition steadiness was checked again by continuously
253 feeding the annular reactor assembled with the photocatalytic bed.
254

255 **3. Results and discussion**

256 *3.1. Photocatalytic oxidation of PCE*

257 *3.1.1. Influence of number of photocatalytic paint coating layers and substrate*
258 *configuration*

259 A blank test without photocatalyst and irradiated by artificial solar light was
260 performed, showing no measurable PCE concentration decrease (data not shown; run 4
261 in Table 3).

262 Sets of xPC1 with 1, 3, 4, 7, 9, 10 and 12 layers were prepared by dip-coating
263 resulting in an increasing weight of photocatalytic paint P: 103.2 mg, 340.7 mg,
264 442.2 mg, 708.1 mg, 943.9 mg, 1022.8 mg, and 1237.4 mg, respectively (see Table 2).

265 Fig. 2a shows that conversion increases as the number of coating layers (n_{layers}) on
266 the cellulose acetate monolith increases up to seven layers, decreasing afterwards (*ca.*
267 38 % for an incident irradiance of 38.4 W_{UV} m^{-2}, measured within 280 – 400 nm: solar
268 UV fraction). As foreseen, higher amount of TiO_2 photogenerates more electron-hole
269 pairs and, consequently, more molecules of PCE can be oxidized. By contrast, above

seven layers (9, 10 and 12 layers) the photocatalytic activity gradually decreases as the number of layers increases.

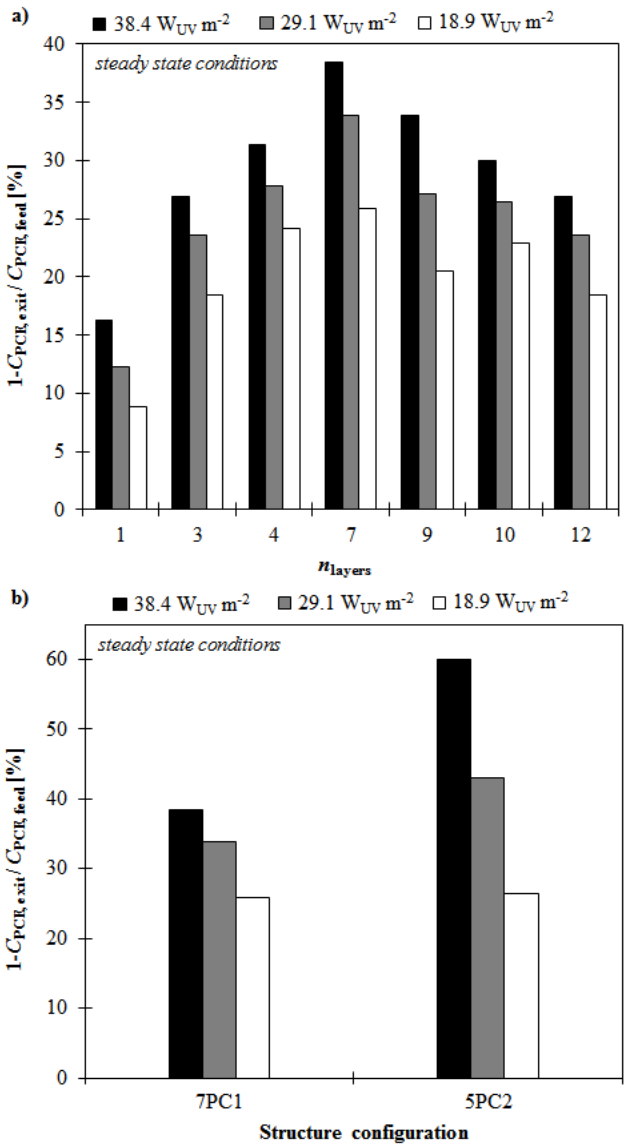

Fig. 2. Influence on photocatalytic conversion of the number of layers under xPC1 configuration (a) and of structure configuration (b) (at steady-state conditions): incident irradiances of 38.4 W_{UV} m^{-2} (■), 29.1 W_{UV} m^{-2} (▩) and 18.9 W_{UV} m^{-2} (□), measured within 280 - 400 nm; $C_{PCE,\ feed}$ = 1100 ppm, Q_{feed}^{*} = 75 cm^3 min^{-1}, and RH^{*} = 40 %; experimental conditions reported in Table 3. * measured at 298 K and 1 bar.

279 This contradictory effect was already described in earlier works [23, 24] and
280 explained by the blockage of the radiation through the photocatalytic film. For this
281 structural configuration (Fig. $1b_1$) thicker coating may create "shadowed" areas where no
282 electron-hole pairs are generated and, consequently, no pollutant molecules are oxidized
283 [25]. As summarized in Table 2, the available area for coating in the PC1 configuration
284 is 806.4 cm^2 whereas for PC2 configuration is 576.0 cm^2 since less walls are available –
285 Fig. $1b_2$. To have a comparable surface density, ρ_A, on both configurations, 5 layers of
286 photocatalytic paint were dip-coated on xPC2. Following the same procedure described
287 in section 2.2 (see Table 2) a set of 5PC2 was prepared.

288 According to SEM analysis on 7PC1 and 5PC2 the photocatalytic paint films were
289 homogeneously coated presenting film thicknesses in the range of 5 – 10 μm (data not
290 shown). The results of both analysis are in line with the previous SEM analysis conducted
291 by the same authors [26].

292 Fig. 2b illustrates the difference in terms of PCE conversion between
293 configuration 1 where the monolith channels are closed and configuration 2 where the
294 channels are open. For the highest irradiance used in this study (38.4 W_{UV} m^{-2}) 5PC2
295 originated a conversion of *ca.* 60 % of PCE against *ca.* 38 % obtained using 7PC1.
296 Decreasing the irradiance from 38.4 W_{UV} m^{-2} to 29.1 W_{UV} m^{-2} the conversion obtained
297 using 5PC2 and 7PC1 configurations diminished 36 % and 21 % respectively, and when
298 the irradiance was decreased to 18.9 W_{UV} m^{-2} the PCE conversion decreased only 2 %.
299 These preliminary results show that under lower irradiances the configuration of the
300 monolithic structure would not affect the photocatalytic activity; instead, using PC2, the
301 higher irradiance employed leads to higher conversions. PC1 has higher surface area
302 available for coating than PC2 but it is worth to note that PC2 has less "shadowed zones",
303 *i.e.* configuration 2 has up to 460.8 cm^2 of surface area free of "shadows" against only

304 230.4 cm^2 of configuration 1. The exposed area to direct radiation and opacity of the
305 structure (under each configuration) may explain the differences in the photocatalytic
306 conversion attained over both configurations.
307
308 *3.1.2. Operating parameters affecting PCE photodegradation*
309 PCE conversion was obtained at steady-state conditions, for five different
310 experimental conditions (Figs. 3-5) using 5PC2 set: (1) feed flow rates of 75, 150, and
311 300 cm^3 min^{-1}, measured at 298 K and 1 bar (Fig. 3; Table 3: runs 1-9); (2) PCE
312 concentrations between 600 and 2200 ppm (Figs. 4; Table 3: runs 4–6 and 10-15); (3)
313 relative humidity of 3, 20 and 40 %, measured at 298 K and 1 bar (Fig. 5; Table 3: runs
314 4-6 and 16-21); (4) relative humidity of 3, 20 and 40 %, measured at 298 K and 1 bar in
315 the absence of oxygen (Fig. 5; Table 3: runs 22-30) (5) incident UV irradiances of
316 38.4 W_{UV} m^{-2} (Figs. 3-5; Table 3: runs 1, 4, 7, 10, 13, 16, 19, 22, 25, and 28),
317 29.1 W_{UV} m^{-2} (Figs. 3-5; Table 3: runs 2, 5, 8, 11, 14, 17, 20, 23, 26, and 29), and
318 18.9 W_{UV} m^{-2} (Figs. 3-5; Table 3: runs 3, 6, 9, 12, 15, 18, 21, 24, 27, 30).
319
320 *3.1.2.1.Effect of feed flow rate*
321 As shown in Fig. 3a, increasing Q_{feed}, from 75 to 300 cm^3 min^{-1} the photocatalytic
322 conversion of PCE decreases up to 73 % depending on the incident irradiance:
323 approximately 60 % of the initial PCE ($C_{PCE,\ feed}$ = 1100 ppm) was converted under
324 I = 38.4 W m^{-2} when the feed flow rates of 75 cm^3 min^{-1} was set while only 16 % of
325 conversion was attained when Q_{feed} = 300 cm^3 min^{-1} was used. On the other hand, higher
326 values of Q_{feed} mean higher loads of PCE per unit of time, which may result in higher
327 mass transfer between the PCE molecules and the catalyst surface. For example,

increasing Q_{feed} from 75 to 150 $cm^3\ min^{-1}$, the PCE photocatalytic rate, r_{PCE}, also increases from 3.58×10^{-5} to 5.13×10^{-5} mol min^{-1}, respectively.

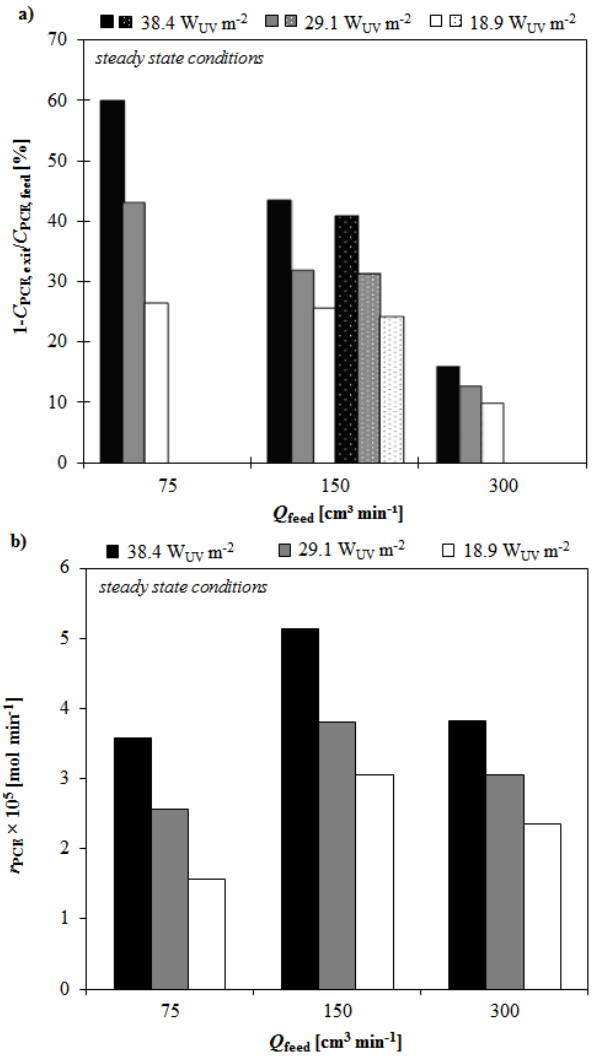

Fig. 3. Effect of feed flow rate [Q_{feed}^*] on PCE conversion (a) and on the PCO reaction rate r_{PCE} (b) at steady-state conditions: experimental points for incident irradiances of 38.4 (■,▩), 29.1 (▩,▨), and 18.9 (□,⊡), measured within 280 - 400 nm; $C_{PCE,\ feed}$ = 1100 ppm, RH^* = 40 %; experimental conditions reported in Table 3. Full coloured columns (■,▩,□) represent 5PC2 first use and dotted columns (▩,▨,⊡) after 50 h under simulated solar radiation and continuous feeding. * measured at 298 K and 1 bar.

338 The results suggest a double antagonistic effect as Q_{feed} increases [27]: i) a
339 decrease in the residence time inside the reactor decreases the adsorption of the pollutant
340 molecules on the paint film surface impairing the efficiency of the PCO process; ii) higher
341 organic load entering the photoreactor enhances the mass transfer between the pollutant
342 molecules and the catalytic film surface resulting in higher PCO reaction rates. However,
343 when Q_{feed} = 300 cm^3 min^{-1} was set, r_{PCE} decreased to 3.82 × 10^{-5} mol min^{-1}. A low
344 residence time (τ = 44 s) together with a high organic load entering the reactor will reduce
345 the adsorption of PCE molecules on the paint film surface and, at the same time, the
346 excess of PCE molecules on the gas stream may block the catalyst surface from receiving
347 radiation which will, subsequently, reduce the reaction rate of PCE.

348 From Figs. 3a and 3b is observed that for lower Q_{feed} (75 cm^3 min^{-1}) the PCO of
349 PCE becomes proportional to the UV irradiance while increasing Q_{feed} the PCE PCO
350 becomes less dependent on I: for 75 cm^3 min^{-1}, the r_{PCE} increased from 1.57 × 10^{-5} to
351 3.58 × 10^{-5} mol min^{-1} corresponding to an enhancement in terms of PCO conversion from
352 26 to 60 % as the irradiance increased from 18.9 to 38.4 W_{UV} m^{-2}; for 300 cm^3 min^{-1} PCO
353 of PCE was enhanced from 10 % (2.36 × 10^{-5} mol min^{-1}) only to 16 %
354 (3.82 × 10^{-5} mol min^{-1}) for the same range of irradiances.

355 Fig. 3a also presents the PCE photocatalytic conversion over 5PC2 after more than
356 50 h (dotted columns) in experiments under simulated solar radiation and continuous
357 feeding (humid air contaminated with PCE). Results show a slight decrease on conversion
358 (< 5 %) after 50 h, suggesting that the system is rather stable regardless the harsh
359 experimental conditions employed.

360

361 *3.1.2.2.Effect of PCE feed concentration*

362 In Fig. 4a is illustrated the effect of PCE feed concentrations on photocatalytic

363 conversion.

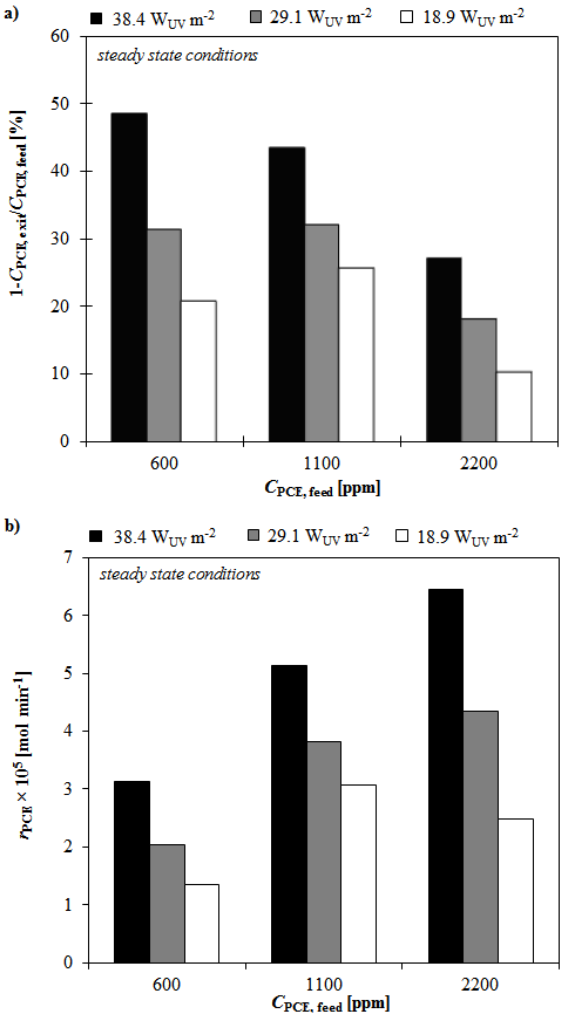

364

365 **Fig. 4** Effect of different concentrations of PCE [$C_{PCE,\ feed}$] on PCE conversion and on the

366 PCO reaction rate r_{PCE}, at steady-state conditions: experimental points for incident

367 irradiances of 38.4 (■), 29.1 (▩), and 18.9 W_{UV} m^{-2} (□), measured within 280 - 400 nm;

368 Q_{feed}^{*} = 150 cm^3 min^{-1} and RH^{*} = 40 %; experimental conditions reported in Table 3.

369 * measured at 298 K and 1 bar.

370

371 Increasing the PCE input molar flow rate to the reactor, less radicals such as
372 hydroxyl ($^{\bullet}OH$) and chlorine ($^{\bullet}Cl$) become available to oxidize the PCE molecules. In
373 fact, for Q_{feed} = 150 cm^3 min^{-1}, decreasing the PCE feed concentration from 2200 ppm to
374 600 ppm, PCE conversion decreased in the range of 42 – 50 % depending on the incident
375 irradiances. However, under lower incident irradiances (29.1 and 18.9 W_{UV} m^{-2}) the PCE
376 conversion increases when $C_{PCE,\ feed}$ increases from 600 to 1100 ppm. This result suggests
377 a possible optimum relation between the residence time inside the reactor and $C_{PCE,\ feed}$ in
378 order to achieve higher PCE conversions through PCO.

379 Regarding the photocatalytic reaction rate of PCE, Fig. 4b shows that for the
380 highest incident irradiance employed (I = 38.4 W_{UV} m^{-2}) the r_{PCE} increases as the $C_{PCE,\ feed}$
381 increases in an almost linear mode. Higher $C_{PCE,\ feed}$ for a same flow rate
382 (Q_{feed} = 150 cm^3 min^{-1}) means higher adsorption in the surface of the photocatalyst, and
383 higher mass transfer between the inlet gas stream and the catalyst surface increasing the
384 PCE photocatalytic reaction rate, r_{PCE}. Decreasing the incident irradiance to 29.1 W_{UV} m^{-}
385 ^{2}, it is observed that the r_{PCE} as a function of $C_{PCE,\ feed}$ does not follow the same trend; the
386 difference between the reaction rates obtained at 1100 ppm and 2200 ppm is smaller.
387 Under I = 18.9 W_{UV} m^{-2} the amount of converted PCE for 2200 ppm of feed
388 concentration is, in fact, lower than that of 1100 ppm. This phenomenon may be justified
389 by the insufficient number of generated photons at lower I. Together with a most likely
390 surface flooding due to an excessive PCE load the PCO reaction rate of PCE is
391 dramatically impaired.
392
393 *3.1.2.3.Effect of water content*
394 Different effects of water content on the performance of TiO_2 based catalysts have
395 been widely reported and are still under debate [28-33]. In the absence of water vapour,

396 the PCO of several chemicals is seriously retarded and their mineralization becomes
397 incomplete; however, excessive water vapour inhibits the degradation by competitive
398 adsorption to the photocatalyst surface [28]. Obee and Brown [29] and Obee and Hay
399 [30] reported that the influence of humidity and contaminant concentrations
400 (formaldehyde, toluene, and 1,3-butadiene) on the oxidation rates on titania surface is due
401 to the competitive adsorption on available hydroxyl adsorption sites and to changes in
402 hydroxyl radical population levels. In addition, the same authors demonstrated that the
403 oxidation rate increases as the humidity decreases (for water content above *ca.*
404 1000 ppm).
405 The effect of humidity on photocatalytic activity was also investigated by Cao et al. [31]
406 using TiO_2-based catalysts for photooxidize 1-butene (1.12×10^{-4} mol m^{-3}). They
407 concluded that in the range 2250 to 12000 ppm (9.22×10^{-2} - 4.92×10^{-1} mol m^{-3}) of water
408 concentration the oxidation rate of 1-butene decreased exponentially with increasing
409 water concentration in the flowing stream.
410 In contrast, Jo and Park [32], Jo et al. [33] works revealed that water content had
411 almost no influence on photo-oxidation of benzene, ethyl benzene, and o-, m-, p-xylenes,
412 trichloroethylene, and perchloroethylene ($\leq 4.10 \times 10^{-6}$ mol m^{-3}). The PCO conversions
413 were close to 100 % for four different RH ranges from 10 % to 100 %
414 (0.10 – 1.03 mol m^{-3}).
415 Fig. 5 shows a reduction of 31 % (from run 4 to run 19) on the PCE conversion
416 under $I = 38.4$ W_{UV} m^{-2} as the water content decreases: 43 % of the initial PCE
417 concentration (1100 ppm or 4.45×10^{-2} mol m^{-3}) was converted when $RH = 40$ %
418 ($C_{H_2O,\ feed} = 3.61 \times 10^{-1}$ mol m^{-3}) and 30 % of PCE was converted when $RH = 3$ %
419 ($C_{H_2O,\ feed} = 2.71 \times 10^{-2}$ mol m^{-3}). Under the lowest irradiance, 18.9 W_{UV} m^{-2}, a similar
420 reduction of PCE conversion is observed: from 26 % to 18 % of converted PCE

421 corresponding to a reduction of 29 % for the same *RH* reduction (from run 6 to run 21).
422 On the other hand, for the lowest *RH* condition (3 %) the concentration of water is lower
423 than that of PCE ($C_{H_2O,\ feed} = 2.71 \times 10^{-2}$ mol m^{-3} and $C_{PCE,\ feed} = 4.45 \times 10^{-2}$ mol m^{-3})
424 which might predicate a dramatic reduction in the PCE conversion. However, such
425 reduction was not observed possibly indicating further mechanisms in the
426 photodegradation of PCE besides the classical attack of hydroxyl radicals. Chlorine
427 radical chain propagation reactions have been a matter of discussion in an attempt to
428 explain the PCO mechanism of chlorinated compounds [28, 34-37]
429

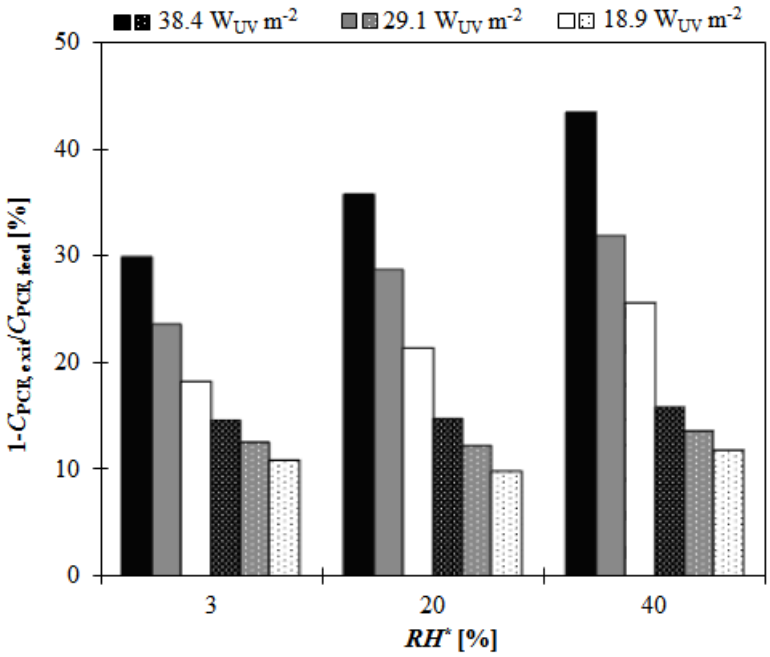

430

431 **Fig. 5.** Effect of water content [RH^*] on PCE conversion at steady-state conditions in the
432 presence of oxygen (full coloured column) and in the absence of oxygen (doted columns):
433 experimental points for incident irradiances of 38.4 (■,▩), 29.1 (▩,▩), and 18.9 W_{UV} m^{-2}
434 (□,⊡), measured within 280 - 400 nm; Q_{feed}^* = 150 cm^3 min^{-1} and $C_{PCE,\ feed}$ = 1100 ppm;
435 experimental conditions reported in Table 3. * measured at 298 K and 1 bar.
436

437 Under the conditions of this study, competitive adsorption of water and PCE
438 molecules on the catalyst surface is unlikely to occur as PCE conversion increases as the
439 water content increases. The possible absence of competition can be related to the PCE
440 higher affinity to the photocatalytic film than that of water or to the high concentrated
441 PCE feed stream even considering the higher content of water at 20 and 40 % of *RH*. In
442 other words, the high input of PCE molecules into the reactor may prevent the water
443 molecules adsorption on the surface of photocatalytic film. However, in our previous
444 work [38], we reported that the PCO of PCE, in similar operational conditions, over
445 PC500 photocatalytic film is impaired at 40 % *RH* indicating a possible competition
446 between PCE and water molecules on the surface of the photocatalytic film. As already
447 pointed out by Obee and Brown [29], a PCO process is a result of the combination of
448 pollutant concentration and water content and depends on the relative affinity of
449 photocatalytic film for the pollutant and water molecules and on the mechanism of the
450 hydroxyl radical attack. Similar ratios of water content/PCE feed concentration are used
451 in both our works, thus the difference in the effect of water on the PCE conversion may
452 be related to material used to prepare the photocatalytic films which may have lower
453 affinity to water and/or PCE molecules reducing their adsorption and, subsequently, the
454 conversion of PCE.
455
456 *3.1.2.4.Effect of oxygen*
457 According to several authors [39-41] the presence of gas-phase molecular oxygen
458 is essential for the photoreaction and increasing the oxygen concentration the pollutant
459 decomposition rate increases. Chang et al. [39] demonstrated that the photocatalytic
460 oxidation rate of acetone increases with the oxygen content; yet, without the presence of
461 molecular oxygen the reaction could still take place. El-Maazawi et al. [40] proposed that

462 in the absence of oxygen the photocatalytic reaction could take place due to the TiO_2
463 lattice oxygen. The oxygen from TiO_2 lattice is depleted during the conversion of gaseous
464 acetone where the role of molecular oxygen from the feed is to replenish the oxygen-
465 deficient surface. However, in an oxygen-free reactor and considering the limited
466 availability of surface lattice oxygen it is expectable that the pollutant conversion would
467 be rather low compared to that found when oxygen is present in the feed stream. It is also
468 expected that depleting oxygen from the TiO_2 lattice would deactivate the catalyst.

469 The dependence of the photoactivity on the gas-phase molecular oxygen absence
470 under different water content conditions is depicted in Fig. 5 (doted columns). The PCE
471 conversion reached similar values for the three *RH* conditions (3, 20 and 40 %):
472 approximately 15, 13 and, 10 % for 38.4, 29.1 and, 18.9 W_{UV} m^{-2}, respectively.
473 Comparing the above values to those obtained for air-flowing experiments, it is observed
474 a reduction in terms of PCE conversion from 54 to 61 % as the water content reduces
475 from 40 to 20 %; for 3 % of *RH* the PCE conversion reduced in the range of 40 to 51 %
476 depending on the employed irradiance.

477 These results suggest a strong contribution of the gas-phase molecular oxygen in
478 the PCO of PCE whereas it is not clear the contribution of the oxygen from the TiO_2
479 lattice. Moreover, considering that TiO_2 PC500 is supported in a paint matrix, it is
480 possible that its components, such as $CaCO_3$ and silicates may, in fact, provide the
481 necessary oxygen to promote photocatalysis in the oxygen-free experiments. On the other
482 hand, hydroxyl radicals, $^{\bullet}OH$, have certainly participation in the initiation of the reaction
483 though they may be not essential to maintain the photocatalytic process as no influence
484 in PCE conversion was observed with the increase of the water content (in the absence of
485 oxygen). As it was already mentioned previously, chlorine radicals chain propagation

reactions may also have a considerably participation in the conversion of PCE. This topic will be discussed in the following sub-section.

3.2. PCE PCO reaction intermediates and pathway

Simultaneously with the study of PCE PCO, a 5 L sampling Tedlar bag was used to collect the outlet gas stream of the reactor, at steady state, during the PCE conversion experiment (run 4 in Table 3). Table 4 summarizes the major intermediate compounds identified and their concentrations were calculated using the response factor of toluene (according to ISO 16000-6 [22]) except for PCE, for which a specific response factor was adopted. The intermediate compounds are not present in the feed gas stream indicating their formation as PCE is converted.

Table 4. Reaction intermediates identified and quantified in the gas-phase photodegradation of PCE (experimental conditions reported in Table 3: run 4)

Compound (i)	CAS Number	Molecular formula	C_i [ppm][a)]	$C_{i,\text{ C-PCE}}$ [ppm]
Perchloroethylene[b)]	127-18-4	C_2Cl_4	6.2×10^2	9.0×10^1
2-chloroacetaldehyde	107-20-0	C_2H_3ClO	3.8×10^{-2}	1.2×10^{-2}
Chloroform	67-66-3	$CHCl_3$	2.0×10^{-1}	2.0×10^{-2}
Carbon tetrachloride	56-23-5	CCl_4	1.5×10^{-1}	1.2×10^{-2}
Ethyl, trichloroacetate	515-84-4	$C_4H_5Cl_3O_2$	3.4×10^{-1}	8.5×10^{-2}
Methyl, trichloroacetate	598-99-2	$C_4H_5Cl_3O_2$	3.4×10^{-1}	8.5×10^{-2}
Pentachloroethane	76-01-7	C_2HCl_5	7.3×10^{-3}	9.0×10^{-3}
Perchloroethane	67-72-1	C_2Cl_6	4.3×10^{-2}	4.4×10^{-2}

[a)] concentration calculated using the response factor of toluene, except for PCE for which specific response factor was used.
[b)] PCE concentration of the feed and exit streams were analysed by MGC: $C_{\text{PCE, feed}}$ = 1100 ppm; $C_{\text{C-PCE, feed}}$ = 159 ppm.

The solar PCO of PCE is initiated with the formation of electron-hole pairs, $e^{-}_{cb}(TiO_2)$ and $h^{+}_{vb}(TiO_2)$ respectively, at the catalyst surface when photons of energy $h\upsilon$ matching or exceeding the TiO_2 band-gap energy are absorbed (eq 2).

$$TiO_2 + h\upsilon \longrightarrow e^{-}_{cb}(TiO_2) + h^{+}_{vb}(TiO_2) \qquad \text{(eq. 2)}$$

Then, the electrons and the holes may react directly with PCE molecules (eq. 3) [42, 43] or with water and oxygen leading to the formation of oxidizing species such as hydroxyl and reducing species such as superoxide radicals [2]. (see eq. 3-6).

$$h^{+}_{vb}(TiO_2) + C_2Cl_4 \longrightarrow C_2Cl_4^{\bullet +} \qquad \text{(eq. 3)}$$

$$h^{+}_{vb}(TiO_2) + H_2O \longrightarrow OH^{\bullet} + H^{+} \qquad \text{(eq. 4)}$$

$$h^{+}_{vb}(TiO_2) + OH^{-} \longrightarrow OH^{\bullet} \qquad \text{(eq. 5)}$$

$$e^{-}_{cb}(TiO_2) + O_2 \longrightarrow O_2^{\bullet -} \qquad \text{(eq. 6)}$$

Several mechanisms of PCE degradation and intermediates have been described in the literature [28, 34-37] and there is still no full agreement. Yamazaki et al. [28] stated that the photocatalytic elimination of PCE may occur via $^{\bullet}OH$ radical or $^{\bullet}Cl$ radical, however the reaction with $^{\bullet}OH$ radical is thermodynamically favourable; furthermore, these authors concluded that $^{\bullet}Cl$ radical initial reaction rarely occurs on the catalyst surface. In opposition, it was suggested that $^{\bullet}Cl$ radical addition to PCE occurs several times faster than $^{\bullet}OH$ radical addition and thus, the $^{\bullet}OH$ radical role in PCO of PCE could be neglected [34, 35]. This conclusion was further substantiated by Lu et al. [36] and Fan and Yates [37] after noting the inactivity of surface $^{\bullet}OH$ groups in the oxidation of methyl chloride and trichloroethylene.

The mechanism proposed in the following schemes relies on the assumption that PCE degradation reaction initiates with the addition of $^{\bullet}OH$ radicals leading to

523 dechlorination reaction where $^{\bullet}Cl$ radicals are formed. Afterwards and based on the
524 nature of the identified compounds within this work, further addition of $^{\bullet}OH$ and/or $O_2^{-\bullet}$
525 radicals will oxidize PCE into 2-chloroacetaldehyde or, alternatively, the addition of $^{\bullet}Cl$
526 radicals may produce chloroalkanes which can be involved in a chain reaction until
527 complete mineralization. Scheme 1 represents the attack of $^{\bullet}OH$ radical to PCE followed
528 by $^{\bullet}Cl$ radical liberation yielding trichloroethenol. The enol could tautomerize to a
529 carbonyl compound such as dichloroacetylchloride (DCAC) and finally producing 2-
530 chloroacetaldehyde and $^{\bullet}Cl$ radical. Although DCAC could not be detected in this study,
531 it has been detected in the degradation of trichloroethylene and perchloroethylene [44,
532 45].

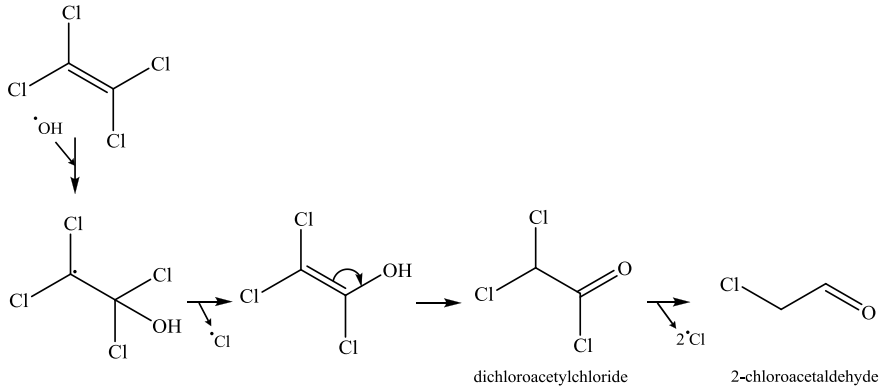

533

534 **Scheme 1.** $^{\bullet}OH$ radical addition to PCE followed by $^{\bullet}Cl$ radical generation.

535

536 The addition of $^{\bullet}Cl$ radicals to PCE (Scheme 2) results in the formation of a very
537 unstable chloroalkyl radical promptly oxidized by superoxide radicals producing a peroxy
538 radical. This radical can be converted into chloroethoxy radical reacting with a second
539 peroxy radical [46] which undergoes a C-C bond scission forming CCl_2O and CCl_3
540 radicals. The latter converts into chloroform or carbon tetrachloride by reacting with H^+
541 or $^{\bullet}Cl$ radical, respectively, while the former produces phosgene that may be hydrolyzed
542 into CO_2 and HCl [28, 47]. Phosgene was not detected in our study, despite of the high
543 $C_{feed,\ PCE}$ (1100 ppm), most likely due to its reaction with water forming the mineralized

final products carbon dioxide and hydrochloric acid [28, 48]. However it has been identified as a reaction intermediate of chlorinated hydrocarbons degradation such as trichloroethylene by several authors [44, 45].

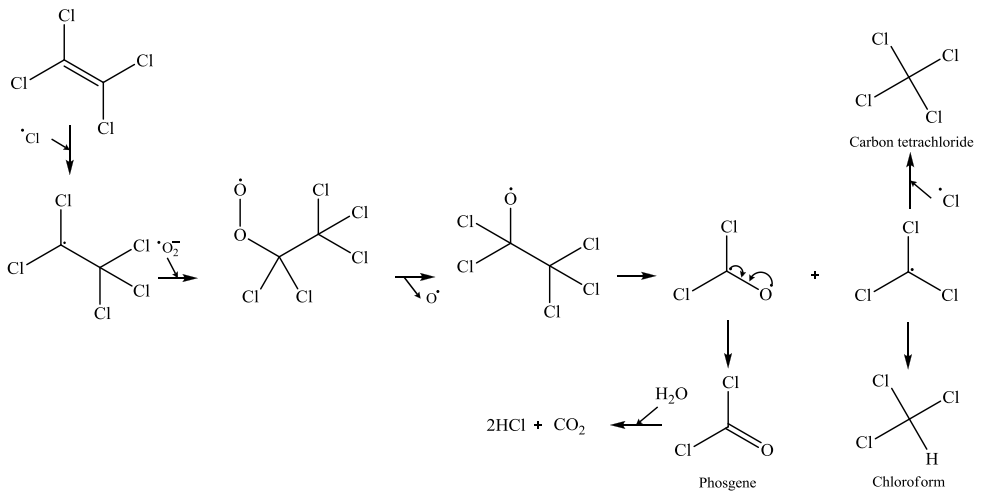

Scheme 2. $^{\bullet}Cl$ radical addition to PCE followed by $O_2^{-\bullet}$ radical addition forming chloroalkanes and phosgene.

Scheme 3 represents the chlorination of PCE producing chloroalkanes. In this case, PCE undergoes the $^{\bullet}Cl$ radical attack producing chloroalkyl radical that can be hydrogenated or chlorinated producing pentachloroethane or perchloroethane, respectively.

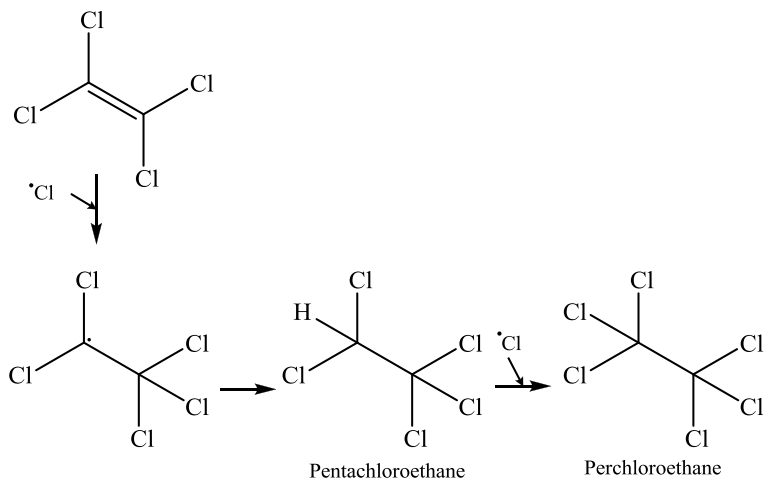

Scheme 3. Chlorination of PCE by addition of $^{\bullet}Cl$ radicals producing chloroalkanes.

Esters derive from the reaction between carboxylic acids and alcohols. Although both kind of compounds were not detected it is possible to schematize a reaction mechanism based on our previous results [21]. In scheme 4 is represented the mechanism of formation of trichloroethyl acetate and trichloromethyl acetate. Both pentachloroethanol and dichloroacetic acid may be formed from the addition of •OH radical to chloroalkyl radical and dichloroacetyl chloride, respectively. The latter may be chlorinated to form trichloroacetic acid. Dichloromethanol can be easily hydrogenated at the surface of the catalyst. Then, from the reactions between trichloroacetic acid and pentachloroethanol or dichloromethanol, ethyl, trichloroacetate and methyl, trichloroacetate may be produced.

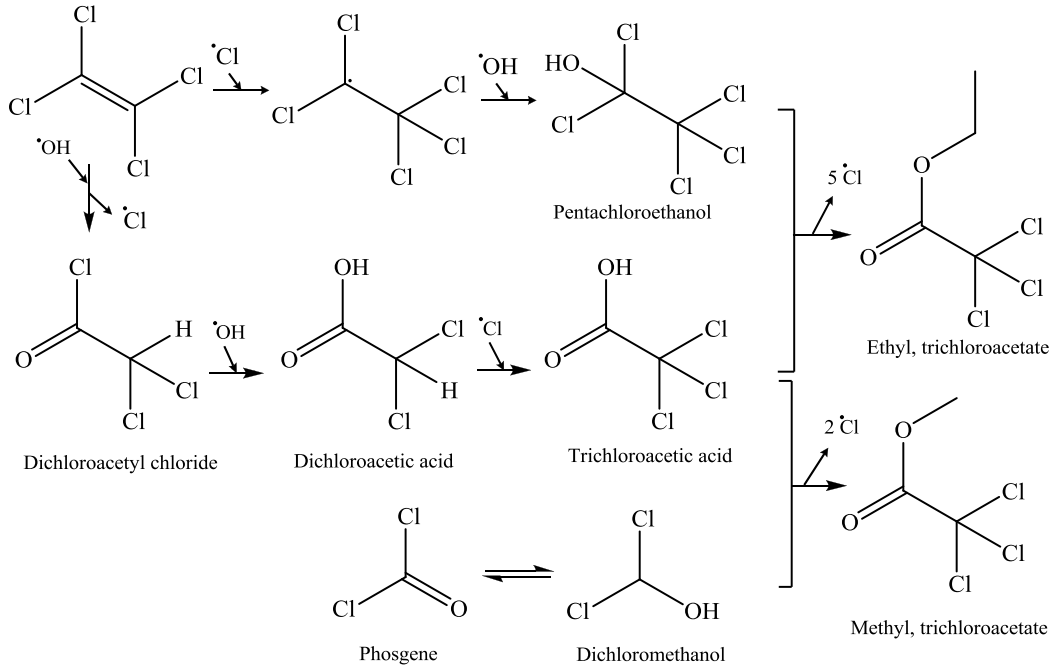

Scheme 4. Esterification of ethyl, trichloroacetate and methyl, trichloroacetate.

The proposed reaction mechanisms are consistent with the data reported in the literature, our previous results and the experimental results obtained in this study. Further well-planned experiments are required to fully understand the role of •OH and •Cl

radicals as well as the evolution of reaction intermediates during degradation through PCO of PCE. Especially, considering the potential formation of highly toxic intermediates such as phosgene, chloroform or carbon tetrachloride in the degradation of chlorinated hydrocarbons such as PCE [44, 45].

It also worth mentioning that the major part of intermediate compounds identified have occupational limit values lower than PCE, which shows that have high toxicity. On the other hand, the concentration of these intermediates is much lower than the initial PCE concentration which compensates its toxicity. For example, chloroform has a limit value of 2 ppm according German Legislation [49], 10 times lower than limit value of PCE which is 20 ppm. The initial concentration of PCE used in this work is 30000 times higher than chloroform.

Considering that $C_{\mathrm{i,\,C\text{-}PCE}}$ refers to the carbon atoms concentration of compound *i* formed from the PCE photodegradation (all unreacted PCE and its major intermediates detected), it can be defined as:

$$C_{\mathrm{i,C\text{-}PCE}} = \frac{C_{\mathrm{i}}}{M_{\mathrm{i}}} \cdot n(\mathrm{C}) \cdot M(\mathrm{C}) \qquad \text{(eq. 7)}$$

where C_{i} [ppm] and M_{i} [g mol^{-1}] are the gas phase concentration and molecular weight of compound *i*, respectively, n(C) is the number of carbon atoms of each component *i* molecule, and M(C) [g mol^{-1}] is the molecular weight of a carbon atom. The mineralization yield (η_{min} in %) can be determined as following:

$$\eta_{\mathrm{min}}[\%] = \left[1 - \frac{\Sigma_{\mathrm{i}}(C_{\mathrm{i,\,C\text{-}PCE}})_{\mathrm{exit}}}{\Sigma_{\mathrm{i}}(C_{\mathrm{i,\,C\text{-}PCE}})_{\mathrm{feed}}}\right] \times 100 \qquad \text{(eq. 8)}$$

Thus, considering the carbon atoms concentration of each identified and quantified degradation intermediates resulting from the PCE molecules conversion, approximately 56 % of PCE remained unreacted, from eq. 8 is possible to conclude that almost complete mineralization into CO_2, H_2O and HCl of the converted PCE was attained. It is worth noting that the mass balance of carbon and chlorine were not

599 confirmed because final products, such as CO_2, HCl, and H_2O, were not quantified.
600 However, photoreactor's feed and exit flow rates were constant, at steady-state. In other
601 words, if PCE or its reaction intermediates were adsorbed on the photocatalytic film
602 surface, at steady state conditions, the amount adsorbed and further desorbed was
603 constant. On the other hand, if intermediates or part of them were being formed instead
604 of CO_2, their concentrations are below the limit of quantification of the GC-MS and,
605 therefore, unable to be measured.
606

607 **4. Conclusions**

608 The lab-scale continuous-flow annular photocatalytic reactor employed in this
609 study for the degradation of PCE over a TiO_2-based paint showed good effectiveness
610 under simulated solar light radiation. Using monolithic structures as substrate for the
611 photocatalytic paint in an annular photoreactor, the operating advantages of a monolithic
612 reactor (simple geometry, much better radiation distribution, low pressure drop and high
613 catalytic surface area per unit of reactor volume) were gathered. The comparison between
614 the two tested substrate configurations (one structure with closed channels and another
615 with open channels) provided interesting results: by removing the outer walls of the
616 substrate (configuration 2), ergo increasing the exposed surface area to radiation the PCE
617 conversion by PCO enhanced up to 56 % depending on the incident irradiance. Using
618 such configuration, it was observed that PCE conversion is greatly affected by the flow
619 rate of the inlet gas stream and initial PCE concentration: increasing four times the feed
620 flow rate (from 75 cm^3 min^{-1} to 300 cm^3 min^{-1}), PCE conversion decreased from 60 % to
621 16 % under 38.4 W_{UV} m^{-2} of irradiance corresponding to a 73 % reduction; in terms of
622 converted PCE load per unit of time it was observed that the highest value was attained
623 for Q_{feed} = 150 cm^3 min^{-1}; for a 3.7-fold increase in PCE feed concentration under

38.4 W_{UV} m^{-2} the converted PCE load also increased although the PCE conversion showed a reduction of 43 % (from 48 % of converted PCE for 600 ppm of PCE feed concentration to 27 % of converted PCE for 2200 ppm of PCE feed concentration). PCE conversion decreased substantially with the decrease of water content in the feed stream, *i.e.* at 3 % of relative humidity the PCE conversion decreased 30 % when compared to the result found at 40 % of relative humidity, however the action of hydroxyl radicals should not be excluded from the photocatalytic mechanism. Removing oxygen from the feed approximately 15 % of PCE conversion corresponding to a reduction in the PCO efficiency up to 56 % depending on the incident irradiance was attained. The reduction of PCE conversion in the absence of oxygen indicates its important role of the gas-phase molecular oxygen in the PCO of PCE whereas it is not clear the contribution of oxygen from the TiO_2 lattice.

Finally, through the monitoring of the reaction products and based on previous works and literature, the reaction mechanisms for heterogeneous photocatalytic oxidation of PCE may consist of a series of reactions involving $^{\bullet}Cl$ radicals, but initiated with the attack of $^{\bullet}OH$ radical generating $^{\bullet}Cl$ radicals.

Acknowledgements

This work was co-financed by FCT/MEC, FEDER under Programe PT2020 (Project UID/EQU/50020/2013). This work was co-financed by QREN, ON2 and FEDER, under Programe COMPETE (Project NORTE-07-0124-FEDER-000015). V.J.P. Vilar and A.M.T. Silva acknowledge the FCT Investigator 2013 Programme (IF/01501/2013 and IF/00273/2013, respectively), with financing from the European Social Fund and the Human Potential Operational Programme. R.A.R. Monteiro and J. Ângelo gratefully

acknowledge FCT for their PhD Research Fellowships, SFRH/BD/69323/2010 and SFRH/BD/79974/2011, respectively.

651 **References**

652 [1] J.-M. Herrmann, Heterogeneous photocatalysis: state of the art and present
653 applications, Top. Catal., 34 (2005) 49-65.
654 [2] M.R. Hoffmann, S.T. Martin, W. Choi, D.W. Bahnemann, Environmental
655 applications of semiconductor photocatalysis, Chem. Rev., 95 (1995) 69-96.
656 [3] M. Kaneko, I. Okura, Photocatalysis: science and technology, Springer, Heidelberg,
657 2002.
658 [4] K. Murugan, R. Subasri, T.N. Rao, A.S. Gandhi, B.S. Murty, Synthesis,
659 characterization and demonstration of self-cleaning TiO_2 coatings on glass and glazed
660 ceramic tiles, Prog. Org. Coat., 76 (2013) 1756-1760.
661 [5] P.S. Marcos, J. Marto, T. Trindade, J.A. Labrincha, Screen-printing of TiO_2
662 photocatalytic layers on glazed ceramic tiles, J. Photochem. Photobiol. A, 197 (2008)
663 125-131.
664 [6] C.S. Poon, E. Cheung, NO removal efficiency of photocatalytic paving blocks
665 prepared with recycled materials, Constr. Build. Mater., 21 (2007) 1746-1753.
666 [7] C.S. Poon, E. Cheung, Performance of photocatalytic paving blocks made from waste,
667 in: Proceedings of the ICE - Waste and Resource Management, 2006, pp. 165-171.
668 [8] J. Zhang, W. Liu, P. Wang, K. Qian, Photocatalytic behavior of cellulose-based paper
669 with TiO_2 loaded on carbon fibers, J. Environ. Chem. Eng., 1 (2013) 175-182.
670 [9] H. Taoda, M. Fukaya, E. Watanabe, K. Tanaka, VOC decomposition by photocatalytic
671 wall paper, Mater. Sci. Forum, 510-511 (2006) 22-25.
672 [10] C.E. Bygott, J.E. Maltby, J.L. Stratton, R. McIntyre, Photocatalytic coatings for the
673 construction industry, in: International RILEM Symposium on Photocatalysis,
674 Environment and Construction Materials, Florence, Italy, 2007, pp. 251-258.

675 [11] C. Águia, J. Ângelo, L.M. Madeira, A. Mendes, Influence of photocatalytic paint
676 components on the photoactivity of P25 towards NO abatement, Catal. Today, 151 (2010)
677 77-83.
678 [12] T. Maggos, J.G. Bartzis, M. Liakou, C. Gobin, Photocatalytic degradation of NO_x
679 gases using TiO_2-containing paint: a real scale study, J. Hazard. Mater., 146 (2007) 668-
680 673.
681 [13] T. Salthammer, F. Fuhrmann, Photocatalytic surface reactions on indoor wall paint,
682 Environ. Sci. Technol., 41 (2007) 6573-6578.
683 [14] J. Ângelo, L. Andrade, A. Mendes, Highly active photocatalytic paint for NO_x
684 abatement under real-outdoor conditions, Appl. Catal. A: Gen., 484 (2014) 17-25.
685 [15] J.V. Teixeira, S.M. Miranda, R.A.R. Monteiro, F.V.S. Lopes, J. Madureira, G.V.
686 Silva, N. Pestana, E. Pinto, V.J.P. Vilar, R.A.R. Boaventura, Assessment of indoor
687 airborne contamination in a wastewater treatment plant, Environ. Monit. Assess., 185
688 (2013) 59-72.
689 [16] R.E. Hayes, S.T. Kolaczkowski, W.J. Thomas, Finite-element model for a catalytic
690 monolith reactor, Comput. Chem. Eng., 16 (1992) 645-657.
691 [17] J. Blanco, S. Malato, P. Fernandez, A. Vidal, A. Morales, P. Trincado, J.C. Oliveira,
692 C. Minero, M. Musci, C. Casalle, M. Brunotte, S. Tratzky, N. Dischinger, K.-H. Funken,
693 C. Sattler, M. Vincent, M. Collares-Pereira, J.F. Mendes, C.M. Rangel, Compound
694 parabolic concentrator technology development to comercial solar detoxification
695 aplications, Sol. Energy, 67 (1999) 317-330.
696 [18] A.V. Vorontsov, E.N. Savinov, G.B. Barannik, V.N. Troitsky, V.N. Parmon,
697 Quantitative studies on the heterogeneous gas-phase photooxidation of CO and simple
698 VOCs by air over TiO_2, Catal. Today, 39 (1997) 207-218.

[19] W.A. Jacoby, D. Blake, R.D. Noble, C.A. Koval, Kinetics of the oxidation of trichloroethylene in air via heterogeneous photocatalysis, J. Catal., 157 (1995) 87-96.

[20] C. Águia, J. Ângelo, L.M. Madeira, A. Mendes, Photo-oxidation of NO using an exterior paint - screening of various commercial titania in powder pressed and paint films, J. Environ. Manage., 92 (2011) 1724-1732.

[21] F.V.S. Lopes, R.A.R. Monteiro, A.M.T. Silva, G.V. Silva, J.L. Faria, A.M. Mendes, V.J.P. Vilar, R.A.R. Boaventura, Insights into UV-TiO_2 photocatalytic degradation of PCE for air decontamination systems, Chem. Eng. J., 204–206 (2012) 244-257.

[22] ISO 16000-6. Determination of volatile organic compounds in indoor and test chamber air by active sampling on Tenax TA sorbent, thermal desorption and gas chromatography using MS or MS/FID, in, 2004.

[23] T.N. Obee, Photooxidation of sub-parts-per-million toluene and formaldehyde levels on titania using a glass-plate reactor, Environ. Sci. Technol., 30 (1996) 3578-3584.

[24] H.T. Chang, N.-M. Wu, F. Zhu, A kinetic model for photocatalytic degradation of organic contaminants in a thin-film TiO_2 catalyst, Water Res., 34 (2000) 407-416.

[25] K.-H. Wang, H.-H. Tsai, Y.-H. Hsieh, The kinetics of photocatalytic degradation of trichloroethylene in gas phase over TiO_2 supported on glass bead, Appl. Catal. B: Environ., 17 (1998) 313-320.

[26] R.A.R. Monteiro, F.V.S. Lopes, A.M.T. Silva, J. Ângelo, G.V. Silva, A.M. Mendes, R.A.R. Boaventura, V.J.P. Vilar, Are TiO_2-based exterior paints useful catalysts for gas-phase photooxidation processes? A case study on *n*-decane abatement for air detoxification, Appl. Catal. B: Environ., 147 (2014) 988-999.

[27] M. Hussain, N. Russo, G. Saracco, Photocatalytic abatement of VOCs by novel optimized TiO_2 nanoparticles, Chem. Eng. J., 166 (2011) 138-149.

723 [28] S. Yamazaki, H. Tsukamoto, K. Araki, T. Tanimura, I. Tejedor-Tejedor, M.A.
724 Anderson, Photocatalytic degradation of gaseous tetrachloroethylene on porous TiO_2
725 pellets, Appl. Catal. B: Environ., 33 (2001) 109-117.
726 [29] T.N. Obee, R.T. Brown, TiO_2 photocatalysis for indoor air applications: effects of
727 humidity and trace contaminat levels on the oxidation rates of formaldehyde, toluene, and
728 1,3-butadiene, Environ. Sci. Technol., 29 (1995) 1223-1231.
729 [30] T.N. Obee, S.O. Hay, Effects of moisture and temperature on the photooxidation of
730 ethylene on titania, Environ. Sci. Technol., 31 (1997) 2034-2038.
731 [31] L. Cao, A. Huang, F.-J. Spiess, S.L. Suib, Gas-Phase Oxidation of 1-Butene Using
732 Nanoscale TiO_2 Photocatalysts, J. Catal., 188 (1999) 48-57.
733 [32] W.K. Jo, K.H. Park, Heterogeneous photocatalysis of aromatic and chlorinated
734 volatile organic compounds (VOCs) for non-occupational indoor air application,
735 Chemosphere, 57 (2004) 555-565.
736 [33] W.-K. Jo, J.-H. Park, H.-D. Chun, Photocatalytic destruction of VOCs for in-vehicle
737 air cleaning, J. Photochem. Photobiol. A, 148 (2002) 109-119.
738 [34] N. Petit, A. Bouzaza, D. Wolbert, P. Petit, J. Dussaud, Photocatalytic degradation of
739 gaseous perchloroethylene in continuous flow reactors: rate enhancement by chlorine
740 radicals, Catal. Today, 124 (2007) 266-272.
741 [35] L.P. Thüner, I. Barnes, K.H. Becker, T.J. Wallington, L.K. Christensen, J.J. Orlando,
742 B. Ramacher, Atmospheric chemistry of tetrachloroethene (Cl_2CCCl_2): products of
743 chlorine atom initiated oxidation, J. Phys. Chem. A, 103 (1999) 8657-8663.
744 [36] G. Lu, A. Linsebigler, J.T. Yates, Photooxidation of CH_3Cl on TiO_2 (110): a
745 mechanism not involving H_2O, J. Phys. Chem., 99 (1995) 7626-7631.

[37] J. Fan, J.T. Yates, Mechanism of photooxidation of trichloroethylene on TiO_2: Detection of intermediates by infrared spectroscopy, J. Am. Chem. Soc., 118 (1996) 4686-4692.

[38] R.A.R. Monteiro, S.M. Miranda, C. Rodrigues-Silva, J.L. Faria, A.M.T. Silva, R.A.R. Boaventura, V.J.P. Vilar, Gas phase oxidation of *n*-decane and PCE by photocatalysis using an annular photoreactor packed with a monolithic catalytic bed coated with P25 and PC500, Appl. Catal. B: Environ., 165 (2015) 306-315.

[39] C.-P. Chang, J.-N. Chen, M.-C. Lu, Heterogeneous photocatalytic oxidation of acetone for air purification by near UV-irradiated titanium dioxide, J. Environ. Sci. Heal. A, 38 (2003) 1131-1143.

[40] M. El-Maazawi, A.N. Finken, A.B. Nair, V.H. Grassian, Adsorption and photocatalytic oxidation of acetone on TiO_2: an *in situ* transmission FT-IR study, J. Catal., 191 (2000) 138-146.

[41] D.S. Muggli, J.L. Falconer, Role of lattice oxygen in photocatalytic oxidation on TiO_2, J. Catal., 191 (2000) 318-325.

[42] F. Benoit-Marquié, U. Wilkenhöner, V. Simon, A.M. Braun, E. Oliveros, M.-T. Maurette, VOC photodegradation at the gas–solid interface of a TiO_2 photocatalyst: Part I: 1-butanol and 1-butylamine, J. Photochem. Photobiol. A, 132 (2000) 225-232.

[43] L. Cermenati, P. Pichat, C. Guillard, A. Albini, Probing the TiO_2 photocatalytic mechanisms in water purification by use of quinoline, photo-fenton generated $OH^{\bullet}$ radicals and superoxide dismutase, J. Phys. Chem. B, 101 (1997) 2650-2658.

[44] M.R. Nimlos, W.A. Jacoby, D.M. Blake, T.A. Milne, Direct mass spectrometric studies of the destruction of hazardous wastes. 2. Gas-phase photocatalytic oxidation of trichloroethylene over titanium oxide: products and mechanisms, Environ. Sci. Technol., 27 (1993) 732-740.

[45] W.A. Jacoby, M.R. Nimlos, D.M. Blake, R.D. Noble, C.A. Koval, Products, intermediates, mass balances, and reaction pathways for the oxidation of trichloroethylene in air via heterogeneous photocatalysis, Environ. Sci. Technol., 28 (1994) 1661-1668.

[46] A.S. Hasson, I.W.M. Smith, Chlorine atom initiated oxidation of chlorinated ethenes: results for 1,1-dichloroethene (H_2CCCl_2), 1,2-dichloroethene (HClCCClH), trichloroethene ($HClCCCl_2$), and tetrachloroethene (Cl_2CCCl_2), J. Phys. Chem. A, 103 (1999) 2031-2043.

[47] P.B. Amama, K. Itoh, M. Murabayashi, Photocatalytic oxidation of trichloroethylene in humidified atmosphere, J. Mol. Catal. A-Chem., 176 (2001) 165-172.

[48] S. Yamazaki-Nishida, X. Fu, M.A. Anderson, K. Hori, Chlorinated byproducts from the photoassisted catalytic oxidation of trichloroethylene and tetrachloroethylene in the gas phase using porous TiO_2 pellets, J. Photochem. Photobiol. A, 97 (1996) 175-179.

[49] GESTIS database (www.dguv.de/ifa/en/gestis/limit_values/index.jsp, last accessed June 2015).